International Journal of Thermal Sciences 49 (2010) 397–408

Contents lists available at ScienceDirect

International Journal of Thermal Sciences

journal homepage: www.elsevier.com/locate/ijts

Heat transfer characteristics during melting of a metal spherical particle in its own liquid

Amitesh Kumar, Subhransu Roy*

Department of Mechanical Engineering, Indian Institute of Technology, Kharagpur 721302, India

ARTICLE INFO

Article history:
Received 29 October 2008
Received in revised form
10 July 2009
Accepted 10 July 2009
Available online 7 August 2009

Keywords:
Forced convection
Heat transfer
Melting
Superheat
Numerical simulation
Stefan number

ABSTRACT

There are manufacturing applications like surface modification and repair technologies where metal particles go into the superheated melt pool heated by an intense heat source and as the workpiece moves away from the energy source this pool solidifies to form a continuous built-up layer. In the present study two-dimensional axisymmetric Navier–Stokes and energy equations are solved using finite volume method to predict the time required for a metal sphere to melt in a melt pool of the same material. The effect of forced convection, characterised by Reynolds number, and superheat of the melt pool, characterised by Stefan number, has been studied in detail for material of different Prandtl numbers. Effect of buoyancy is neglected for the present investigation. It is found that the effect of convection on melting time is more pronounced if $RePr/Ste^{2/3}$ is high. The rate of melting of the metal sphere with time under different conditions is also presented. Finally, the heat transfer characteristic is represented by the correlation of Nusselt number with Reynolds number, Stefan number and Prandtl number.

1. Introduction

There are manufacturing applications like cladding, surface alloying and other surface repair technologies where metal powder particles of radius 10–100 μm are injected into the superheated melt pool under intense energy source with velocity in the range of 0.1–10 m/s. The powder particles melt and mix with the surrounding liquid. The rate of melting of these particles depends on the rate of heat transfer from the surrounding superheated liquid. It is important to study the heat transfer characteristics of these melting particles and the factors that influence this heat transport.

There are a few studies on the melting dynamics of non-metallic spheres at different convective regimes. Kranse and Schenk [1] performed experiments on free convection melting of a submerged benzene sphere in an excess amount of its own liquid ($Pr = 8.3$ and $10^8 < Gr_D < 10^9$). The results provided an equation for the Nusselt number in terms of the Grashof and Prandtl numbers. Schenk and Schenkels [2] have considered melting of an ice sphere in water, the uniform temperature of which is varied between 0 °C and 10 °C, under free convection regime. They accounted for the effect of convection inversion due to the anomalous behaviour of thermal expansion coefficient of the water near water temperature of 4 °C. [3] visualised melting of a wax sphere in hot water and calculated the melting rate using a simple theoretical analysis which estimates melt layer thickness and heat flux from the fluid. The qualitative and quantitative analyses of melting process of ice spheres have been performed experimentally by [4,5] under forced and mixed convective regimes. They calculated the time variations of local melting rate, local heat transfer coefficient and local Nusselt number at different angular positions by recording the change of shape of the melting ice spheres with time at different velocities and supply temperatures of water for different initial temperatures of ice. They have also given a correlation relating average Nusselt number to Reynolds number, Grashof number, Prandtl number and Stefan number for $80 \le Re_D \le 3200$, $0.0016 \le Gr_D/Re_D^2 = 6.98$, $7.91 \le Pr \le 12.69$ and $0.05 \le Ste \le 0.39$ (Gr_D and Re_D are Grashof and Reynolds number based on initial diameter of the sphere).

Melting of a metal spherical particle in a superheated fluid of same or different materials has been studied extensively. Kreith et al. [6] performed an experimental and theoretical investigation of rotating metallic spheres in liquid mercury and suggested a correlation for forced convection. Hsu [7] has given expression for the theoretical Nusselt number for the cases of heat transfer to liquid metals flowing past a single sphere, and past an elliptical rod considering potential flow around the solid object. Anselmo et al. [8] have presented the theoretical and experimental results on the melting of both fully and partially immersed silicon spheres.

* Corresponding author. Tel.: +91 3222 282968.
E-mail address: suroy@iitkgp.ac.in (S. Roy).

1290-0729/$ – see front matter © 2009 Elsevier Masson SAS. All rights reserved.
doi:10.1016/j.ijthermalsci.2009.07.011

Nomenclature

Symbols

A	Porosity function (kg/m^2 s)
f_l	liquid fraction
h	specific sensible enthalpy (J/kg)
H_c	heat transfer coefficient (W/m^2 °C)
L	specific latent heat of fusion (J/kg)
k	thermal conductivity (W/m °C)
Nu	Nusselt number
p	pressure (N/m^2)
Pr	Prandtl number
R	radius of solid sphere (m)
Re_D	Reynolds number based on diameter
Re	Reynolds number
r, z	cylindrical coordinate system (m)
Ste	Stefan number
t	time (s)
U_∞	free stream velocity along z-direction (m/s)
v_r, v_z	velocity component in r, z-direction (m/s)
$\mathbf{V}$	velocity vector (m/s)

Greek symbols

α	thermal diffusivity (m^2/s)
ν	kinematic viscosity (m^2/s)
ψ	stream function (kg/s)
ρ	density (kg/m^3)
τ	dimensionless time

Subscript

b	boiling
∞	free stream condition
l	liquidus
0	initial condition i.e., at $t = 0$
s	solidus or solid

Superscript

*	dimensionless variable

Numerical and experimental investigations on the melting time of solid sphere immersed in liquid aluminium and steel have been carried out by Argyropoulos and Mikrovas [9], Argyropoulos et al. [10]. They have given correlations for forced and natural convection based on the measurement of the melting times of the spheres. More recently Melissari and Argyropoulos [11,12] have conducted an extensive numerical and experimental analyses of the melting of pure aluminium and AZ91 magnesium alloy in the liquid bath of same material. They found out the melting time of the immersed sphere by recording the change in electrical resistance between the tip of a wire inside the sphere and the bath. In another paper [13] found the correlation for forced convection heat transfer by correlating the Nusselt number to Reynolds and Prandtl numbers. Although they have considered a wide range of fluids with different Prandtl numbers for simulation but the study was limited to small values of Stefan number signifying the low superheat ($\leq$100 °C) of the surrounding liquid. However in practice (e.g. laser cladding process) surrounding fluid temperature can go close to evaporation temperature resulting in higher value of Stefan number. Therefore, it is extremely important to study the effect of Stefan number on the heat transfer characteristics.

The purpose of the present investigation is to develop a mathematical model to study heat transfer characteristics of metal particles under a large range of superheat of the surrounding liquid, a range of surrounding liquid velocities and Prandtl numbers. A heat transfer correlation has been developed for different Reynolds number, Stefan numbers and Prandtl numbers. The role of Stefan number is important, because it affects the flow characteristic significantly, and very little information is available in the literature.

2. Mathematical model

The physical model considered for the present study is that of a solid sphere of initial radius R_0 which is kept at temperature very close to the solidus temperature of the material. The solid sphere is exposed to a superheated melt with inflow velocity U_∞. Melting will take place at the surface and solid–liquid interface will move into the solid. Emphasis is placed on analysis of constrained melting which means that both solid and liquid have the same density. The surrounding fluid is the molten phase of the same material. The schematic diagram is shown in Fig. 1.

2.1. Governing equations

The flow around the melting sphere is considered to be laminar as the Reynolds number is kept within 10^3 which is two orders of magnitude lower than the critical Reynolds number of 3×10^5 beyond which isothermal flow around a solid sphere turns turbulent [14]. Axisymmetric flow of Newtonian and incompressible fluid is considered.

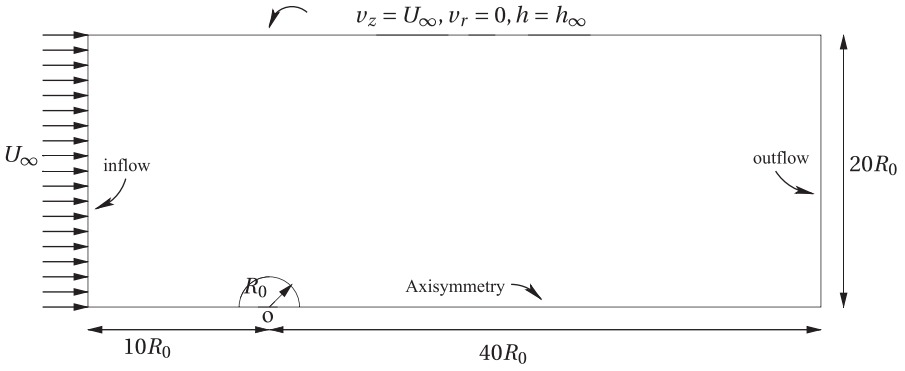

Fig. 1. Schematic diagram of melting of a sphere under forced convection.

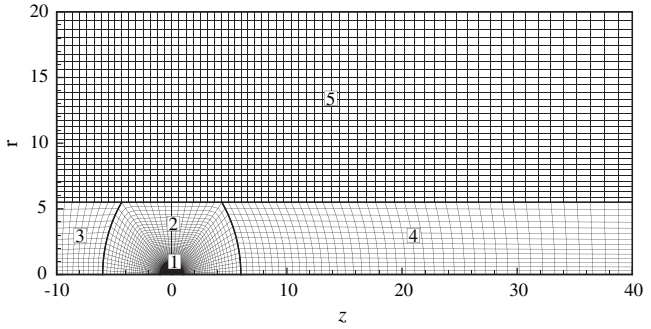

Fig. 2. Two-dimensional axisymmetric computational grid for the melting particle.

The minimum inflow velocity U_∞ can be zero. Therefore U_∞ is not a good scaling variable; instead a scaling velocity is found by making $\mathrm{Re}\,\mathrm{Pr}=1$ giving α/R_0, the heat diffusion speed, as a scaling velocity. With this new velocity scale, the non-dimensional parameters are:

$$r^\star = \frac{r}{R_0} \quad z^\star = \frac{z}{R_0} \quad v_r^\star = \frac{v_r}{\alpha/R_0} \quad v_z^\star = \frac{v_z}{\alpha/R_0} \quad \tau = \frac{\alpha t}{R_0^2}$$

$$\mathrm{Re} = \frac{U_\infty R_0}{\nu} \quad p^\star = \frac{p}{\rho\alpha^2/R_0^2} \quad h^\star = \frac{h-h_s}{h_\infty - h_s}$$

$$\mathrm{Ste} = \frac{h_\infty - h_s}{L} \quad \mathrm{Pr} = \frac{\nu}{\alpha}$$

Non-dimensional Navier–Stokes equations along with energy transport equation are presented. The dimensionless variables are distinguished from their dimensional counterparts by superscript *.

$$\nabla^\star \cdot \mathbf{v}^\star = 0 \tag{1}$$

$$\frac{\partial v_r^\star}{\partial \tau} + (\mathbf{v}^\star \cdot \nabla^\star) v_r^\star = -\frac{\partial p^\star}{\partial r^\star} + \mathrm{Pr}\left(\nabla^{\star 2} v_r^\star - \frac{v_r^\star}{r^{\star 2}}\right) + A^\star v_r^\star \tag{2}$$

$$\frac{\partial v_z^\star}{\partial \tau} + (\mathbf{v}^\star \cdot \nabla^\star) v_z^\star = -\frac{\partial p^\star}{\partial z^\star} + \mathrm{Pr}\nabla^{\star 2} v_z^\star + A^\star v_z^\star \tag{3}$$

$$\frac{\partial h^\star}{\partial \tau} + (\mathbf{v}^\star \cdot \nabla^\star) h^\star = \nabla^{\star 2} h^\star - \frac{1}{\mathrm{Ste}}\left(\frac{\partial f_l}{\partial \tau} + (\mathbf{v}^\star \cdot \nabla^\star) f_l\right) \tag{4}$$

Non-dimensional boundary conditions are:

Upstream $0 \le r^\star \le 20,\ z^\star = -10:\ v_r^\star = 0,\ v_z^\star = \mathrm{RePr},\ h^\star = 1$

Downstream $0 \le r^\star \le 20,\ z^\star = 40:\ \frac{\partial v_r^\star}{\partial z^\star} = 0,\ \frac{\partial v_z^\star}{\partial z^\star} = 0,\ \frac{\partial h^\star}{\partial z^\star} = 0$

Axis $r^\star = 0,\ -10 \le z^\star \le 40:\ v_r^\star = 0,\ \frac{\partial v_z^\star}{\partial r^\star} = 0,\ \frac{\partial h^\star}{\partial r^\star} = 0$

Lateral free stream $r^\star = 20,\ -10 \le z^\star \le 40:\ v_r^\star = 0,\ v_z^\star = \mathrm{RePr},\ h^\star = 1$

Non-dimensional initial conditions are:

Solid sphere : $h^\star = 0,\quad v_r^\star = v_z^\star = 0$

Surrounding fluid : $h^\star = 1,\quad v_r^\star = v_z^\star = 0$

It is to be noted that the free stream velocity boundary condition $v_z^\star = \mathrm{RePr}$ is implemented through the use of a Reynolds number. To solve the energy equation, single region (or continuum) enthalpy formulation is implemented. A Darcy law type porous medium formulation, due to Voller and Prakash [15], is utilised to account for the effect of phase change on convection. The last term in the momentum equations (2) and (3) is Darcy damping term $A^\star$ which smoothly connects the solid region

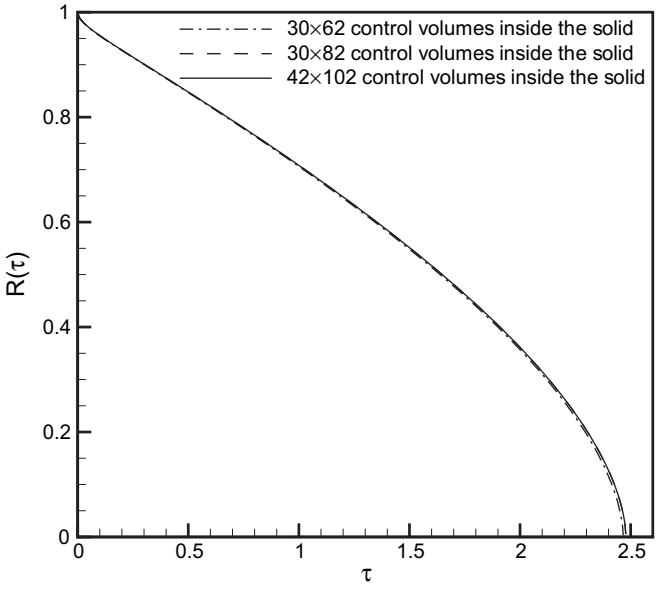

Fig. 3. Variation of non-dimensional effective radius with time for $\mathrm{Pr}=0.01$, $\mathrm{Ste}=0.1$ and $\mathrm{Re}=1000$.

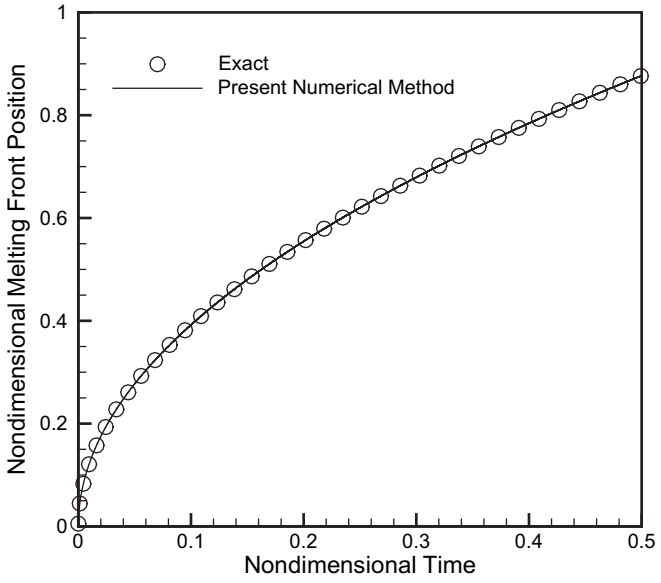

Fig. 4. Comparison between the present numerical method and the exact solution for $\mathrm{Ste}=1$.

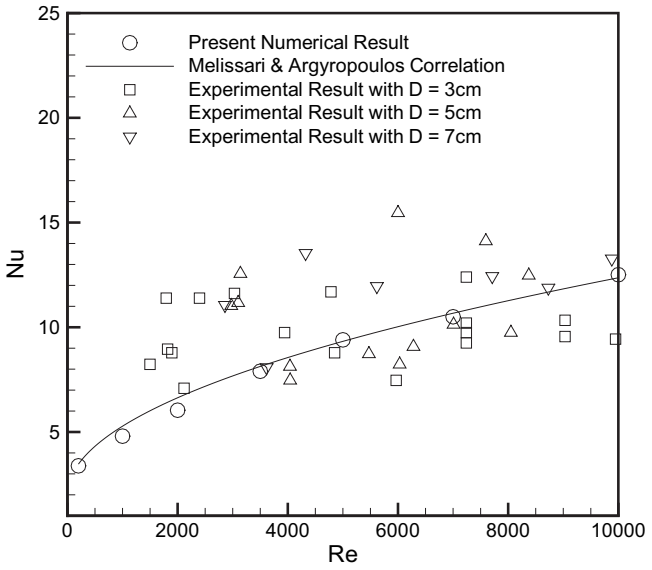

Fig. 5. Nusselt number results for melting of aluminium sphere in a 60 °C superheated molten aluminium.

(having zero velocity and infinite viscosity) to the liquid metal (having vigorous convection and finite viscosity) through the mushy region. This porosity function is defined as [16],

$$A^{\star} = \frac{-C_0^{\star}(1-f_l)^2}{f_l^3}, \quad C_0^{\star} = \frac{C_0 R_0^2}{\rho_0 \alpha_0} \tag{5}$$

where $C_0 = 1.016 \times 10^6$ kg/s m^3. The liquid fraction in the mushy region around the melting interface is calculated using linear model which is given as follows.

pure solid, $h^{\star} \le 0$: $f_l = 0.0$

mushy region, $0 \le h^{\star} \le h_l^{\star}$: $f_l = \dfrac{h^{\star}}{h_l^{\star}}$

pure liquid, $h^{\star} \ge h_l^{\star}$: $f_l = 1.0$

During melting the effective radius $R^*(\tau)$ of the solid was calculated based on the instantaneous volume $\Omega^*(\tau)$ of the solid as

$$R^{\star}(\tau) = \left(\frac{3\Omega^{\star}(\tau)}{4\pi}\right)^{1/3}, \quad \text{where,} \quad \Omega^{\star}(\tau) = \int_{\Omega} (1-f_l)\mathrm{d}\Omega^{\star}$$

A Nusselt number for the melting solid during start of melting when the radius is R_0 is derived in the Appendix. It can be expressed in terms of the non-dimensional melting time $\Delta\tau_{melt}$ of the solid and the Stefan number as shown below.

$$\mathrm{Nu} = \frac{2}{3\mathrm{Ste}\Delta\tau_{melt}} \tag{6}$$

Table 2
Non-dimensional total time of melting for diffusion-controlled melting i.e., Re = 0.

Ste	0.025	0.05	0.1	0.25	0.5	1.0	1.5	2.0
$\Delta\tau_{melt}$	17.954	8.700	4.211	1.640	0.834	0.452	0.328	0.267

2.2. Solution approach

The two-dimensional axisymmetric Navier–Stokes equation along with energy equation have been discretised on a structured collocated, non-orthogonal multiblock grid system using finite volume approach. The grid with five structured blocks used for this simulation is shown in Fig. 2. The governing equations were solved using SIMPLE algorithm of Patankar [17]. The computational domain size used depends not only on the size of the sphere but also on the condition to which the sphere is exposed. As we are also solving the case of pure conduction; to impose the free stream boundary conditions, upstream, downstream and cross stream distances are taken equal to ten, forty and twenty times respectively of the initial radius. A multiblock grid system having five blocks of 42×102, 42×45, 14×9, 14×42 and 65×28 was found to be sufficient to resolve the details of flow, temperature fields and the liquid–solid interface positions based on comparison of the streamline contours, iso-enthalpy contours and liquid–solid interface positions for various grid densities inside the solid. For example, Fig. 3 shows the variation of non-dimensional radius with time for different grid densities inside the solid. The convergence of the result with the increasing number of control volumes can be seen in the plot. The convective term in the governing equations is discretised using deferred correction approach which gives second order accuracy. The diffusive term and the unsteady term are discretised using central difference scheme and implicit three time level method (a quadratic backward approximation) respectively giving second order accuracy in space and time. Detailed discussion about implicit three time level scheme and the structured multiblock system adopted here can be found in Ferziger and Peric [18].

2.3. Code validation

In order to validate the present numerical model two test cases have been considered and results are compared with the established solution found in the literature. While first test case checks the accuracy of the present numerical method against an exact solution, second one compares the numerical predictions against a published experimental results.

2.3.1. Melting in a semi-infinite domain

A solid, $x \ge 0$, initially at the melting temperature T_m is considered [19]. Surface of the solid at $x = 0$ is raised to a temperature T_w ($>T_m$) at time $t = 0$ and maintained at this constant value for times $t > 0$. Thus melting starts at the surface and the melting front moves in the positive x-direction. Being at the uniform temperature T_m throughout, there is no heat transfer in the solid phase. Only diffusion-controlled phase change with constant thermo-physical properties values have been considered for this purpose. The exact solution for the position of the melting front is given by

Table 1
Thermo-physical properties of some metals at melting point, SI units [21,20].

Material	ρ	μ	c	k	T_l	T_b	$h_l - h_{25^\circ C}$	L
Iron	7.03×10^3	5.6×10^{-3}	824	36	1538	2860	1050×10^3	247×10^3
Nickel	7.85×10^3	4.7×10^{-3}	734	69	1455	2915	1109×10^3	298×10^3
Copper	7.96×10^3	4.0×10^{-3}	495	165.6	1083	2560	670×10^3	208.7×10^3

Table 3
Effect of Re, Pr and Ste on non-dimensional total time of melting.

Ste	$\Delta\tau_{melt}$ for following Re values					
	1.0×10^2	2.5×10^2	5.0×10^2	7.5×10^2	1.0×10^3	Pr
0.025	16.220	13.050	11.500	9.530	9.160	0.01
0.025	11.690	8.625	6.544	5.413	4.648	0.05
0.025	8.946	6.171	4.301	3.458	2.946	0.13
0.05	8.120	6.350	5.900	5.123	4.720	0.01
0.05	5.976	4.332	3.368	2.825	2.392	0.05
0.05	4.572	3.160	2.209	1.775	1.514	0.13
0.1	4.060	3.365	3.074	2.651	2.470	0.01
0.1	3.106	2.293	1.772	1.504	1.262	0.05
0.1	2.381	1.654	1.160	0.931	0.793	0.13
0.25	1.620	1.405	1.355	1.236	1.116	0.01
0.25	1.362	0.985	0.799	0.642	0.572	0.05
0.25	1.059	0.742	0.523	0.420	0.357	0.13
0.5	0.831	0.801	0.754	0.692	0.643	0.01
0.5	0.756	0.549	0.465	0.379	0.334	0.05
0.5	0.607	0.429	0.303	0.244	0.207	0.13
1.0	0.452	0.443	0.434	0.405	0.388	0.01
1.0	0.435	0.335	0.289	0.243	0.211	0.05
1.0	0.369	0.264	0.188	0.152	0.129	0.13
1.5	0.328	0.324	0.322	0.307	0.296	0.01
1.5	0.322	0.256	0.226	0.192	0.168	0.05
1.5	0.284	0.206	0.148	0.121	0.103	0.13
2.0	0.267	0.265	0.264	0.256	0.247	0.01
2.0	0.264	0.239	0.192	0.176	0.146	0.05
2.0	0.239	0.176	0.128	0.104	0.089	0.13

$$s(t) = 2\gamma\sqrt{\alpha t}$$

where γ is the solution of transcendental equation

$$\gamma e^{\gamma^2} erf(\gamma) = \frac{c_p(T_w - T_m)}{L\sqrt{\pi}}$$

For numerical purpose the semi-infinite domain is considered to be of finite length l_{solid}. The thermo-physical properties of the solid, T_w and T_m are chosen in such a way that Stefan number $Ste = c_p(T_w - T_m)/L = 1$. l_{solid} and l^2_{solid}/α are taken as the normalising parameters for length and time respectively. The computed non-dimensional melting front position with non-dimensional time is shown in Fig. 4 for $Ste = 1$. It can be seen from the plot that results obtained by the present numerical method compare very well with the exact solution.

2.3.2. Melting of an aluminium sphere under forced convection

The two-dimensional laminar axisymmetric code on non-orthogonal grid has been validated against the experimental and numerical results of melting of an aluminium sphere under forced convection in an enclosure by Melissari and Argyropoulos [13]. Although they have considered spheres of different materials, different diameters and different initial conditions but we have chosen results of immersion of aluminium spheres initially at room temperature of 20 °C in a 60 °C superheat bath for comparison. For calculating the dimensionless numbers constant thermo-physical property of Aluminium at its liquidus temperature is considered [20]. For a 60 °C superheat, Stefan number turns out to be equal to 0.178. For comparison Reynolds number Re is varied between 200 and 10,000. Fig. 5 shows the comparison between the numerical prediction and the experimental result by Melissari and Argyropoulos. It is to be noted here that these results are presented for Nusselt number and Reynolds number based on the initial diameter D of the sphere denoted by Nu_D and Re_D respectively. The experimental results are scattered but the matching of present computed results with the computed results of Melissari and Argyropoulos [13] for this large range of Re_D and small Ste is good.

3. Results and discussion

The mathematical model was used to study melting of a solid sphere under diffusion-control with static surrounding fluid (i.e., $Re = 0$) and melting under forced convection due to flow in the surrounding fluid. The melting time and the rate of melting were studied. The streamline pattern and the enthalpy field around the melting solid are also presented. The thermo-physical properties of some common metals at the melting temperature given in Table 1 are used as reference properties to evaluate the range of dimensionless parameters. It was found that thermo-physical properties of common metals beyond the melting point are very scarce; and if available, it may go only up to 200–300 °C beyond the melting point [21,20]. In this temperature range of 200–300 °C beyond the melting point the thermal conductivity of common metals can vary by as much as 5% and the dynamic viscosity can decrease by as much as 25%. We have considered the case of melting a metal spherical particle in its molten pool during laser cladding process where metal particles of radius 10–100 μm are injected into the melt pool with a velocity in the range 0.1–10.0 m/s. Taking a typical value of Iron particles having radius 100 μm, velocity 10.0 m/s, density 7.03×10^3 kg/m^3 and viscosity 5.6×10^{-3} Ns/m^2 Reynolds number turns out to be equal to 1.255×10^3. Therefore, in the present study we have gone up to $Re = 10^3$.

3.1. Total time of melting and rate of melting

In diffusion-controlled melting the solid particle remains a perfect sphere at all times with radius decreasing with the passage of time. Table 2 gives the non-dimensional total time of melting for the diffusion-controlled melting at $Re = 0$. In diffusion-controlled melting the fluid is stationery and energy equation (4) is the only governing equation that is solved with appropriate enthalpy boundary conditions and therefore Prandtl number Pr does not play a role. The total time of melting is only a function of Stefan number Ste.

To study the effect of convection, numerical simulations were performed for five Reynolds numbers, three Prandtl numbers and eight Stefan numbers (maximum value of Stefan number is limited by the boiling point of the liquid metal). The total time of melting for different cases considered in the present study is summarised in Table 3. It is found that total time of melting decreases with increase in Reynolds number, Prandtl number and Stefan number. With increase in Reynolds number and Prandtl number convective heat transfer increases which results in faster melting of solid particle. Also by increasing Stefan number the superheat of the surrounding fluid increases promoting conduction heat transfer; as a consequence solid particle melts faster.

The Nusselt number for the sphere having initial radius R_0 is expressed in terms of the total time of melting and the Stefan number as shown in equation (6). By performing the least square fitting of the computed values, a correlation between Nusselt number, Stefan number, Reynolds number and Prandtl number is presented in the range $0.025 \le Ste \le 2.0$, $0 \le Re \le 1.0\times10^3$ and $0.01 \le Pr \le 0.13$. The resultant correlation is given by equation (7) with a standard deviation $\sigma_{corr} = 1.74\%$ and correlation coefficient = 0.997 on 140 degrees of freedom.

$$Nu = \frac{2}{3Ste\Delta\tau_{melt}} = \left(1.26 + \left(-0.916 + Ste^{-0.061}\right)Re^{3/4}Pr^{2/3}Ste^{1/4}\right)Ste^{-0.065} \quad (7)$$

From this correlation it is observed that $\Delta\tau_{melt}$ decreases approximately as $Re^{3/4}$, $Pr^{2/3}$ and $Ste^{5/4}$.

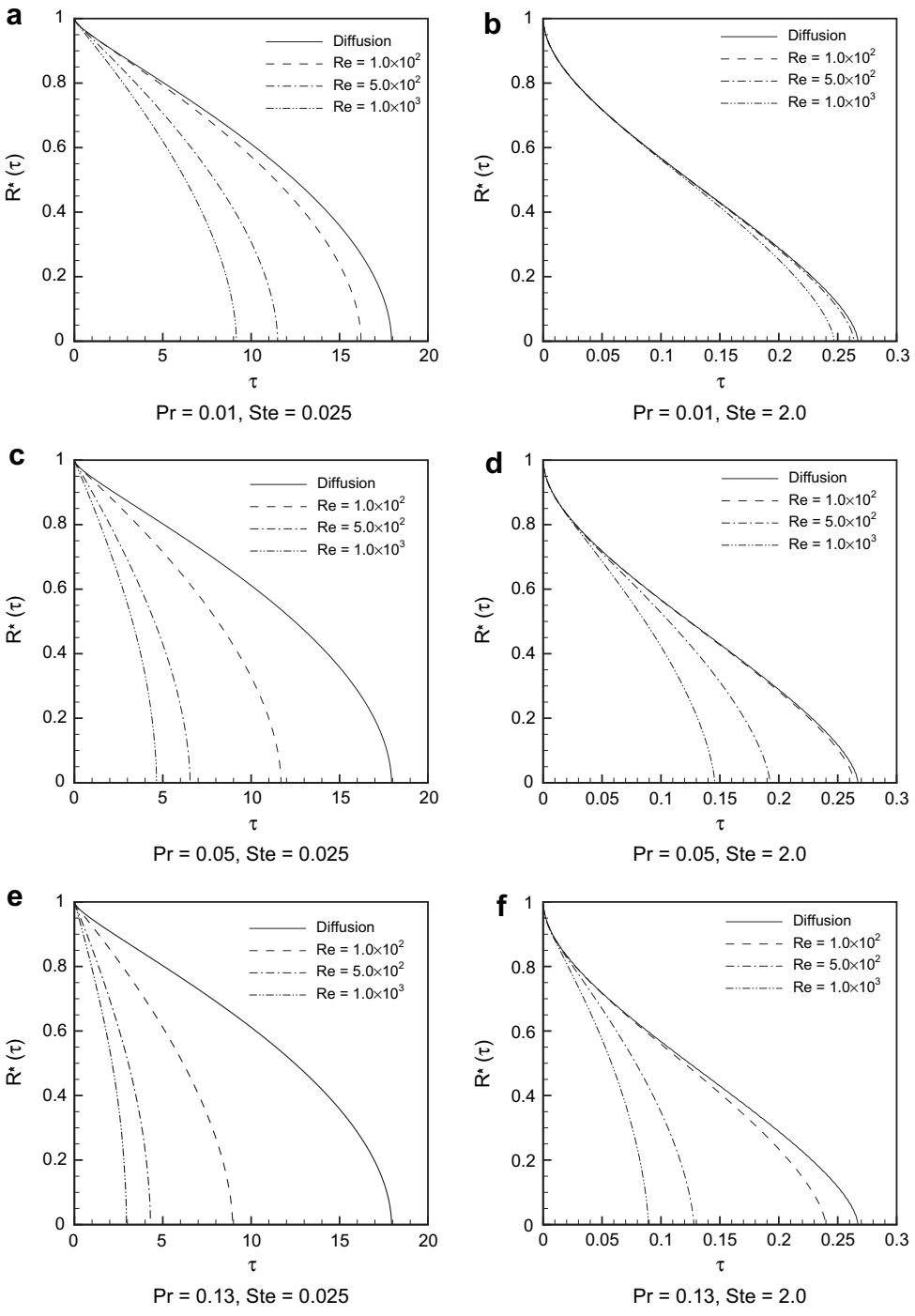

Fig. 6. Variation of non-dimensional effective radius with non-dimensional time.

During melting with convection the particles do not remain spherical, therefore the effective radius based on volume was calculated during melting. Fig. 6 shows the decrease of dimensionless effective radius with dimensionless time during melting for Stefan number of 0.025 and 2.0, for three different Reynolds numbers (100, 500, 1000) and three different Prandtl numbers (0.01, 0.05 and 0.13). The total melting time is maximum for $Re = 0$ i.e., diffusion case and it decreases with increase in Reynolds number and Prandtl number as depicted in Fig. 6. But if $RePr/Ste^{2/3}$ is less than 5 then melting rate approaches within 5% of the respective diffusion case showing negligible role of convection on total time of melting as evident from Fig. 7. In Fig. 6(b) the four curves are for $RePr/Ste^{2/3} = 0$, 0.63, 3.14, 6.3 and they are close to the diffusion case of $Re = 0$. If the time is replaced with fraction time of melting $\tau/\Delta\tau_{melt}$ then the effective radius of solid verses fraction of melt time plot becomes very close to the plot for diffusion case as shown in Fig. 8.

3.2. Streamline and enthalpy field during melting

During melting with forced convection the rate of melting differs in the upstream and downstream region and the particle no

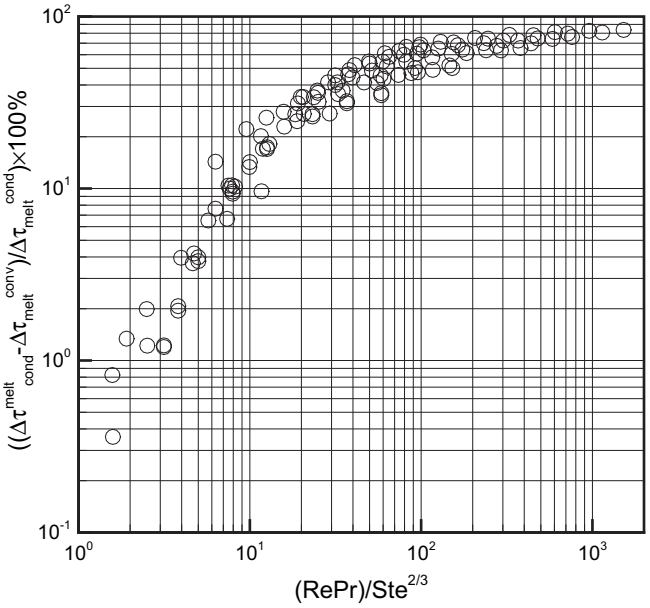

Fig. 7. Deviation in total time of melting from conduction limit.

longer remains a sphere. In the upstream region convection always aids diffusion heat transfer but it is not always so in the downstream region where recirculation takes place at the wake. In a two-dimensional axisymmetric plane the streamline, enthalpy field around the solid and the shape of the particle during melting are presented for Reynolds number of 100, 1000, Prandtl numbers of 0.01, 0.05, 0.13 and Stefan numbers of 0.025, 2.0. The original position of the sphere is denoted by dash–dotted semi-circle with centre (0,0) and dimensionless radius 1; and the shaded area indicates the solid phase at a given instant bounded by line of dimensionless enthalpy contour $h=0$ representing phase change condition. Comparing the shaded region to the original particle position one can find the amount of melting in different directions. In streamlines contours, clockwise recirculation is denoted by dashed lines.

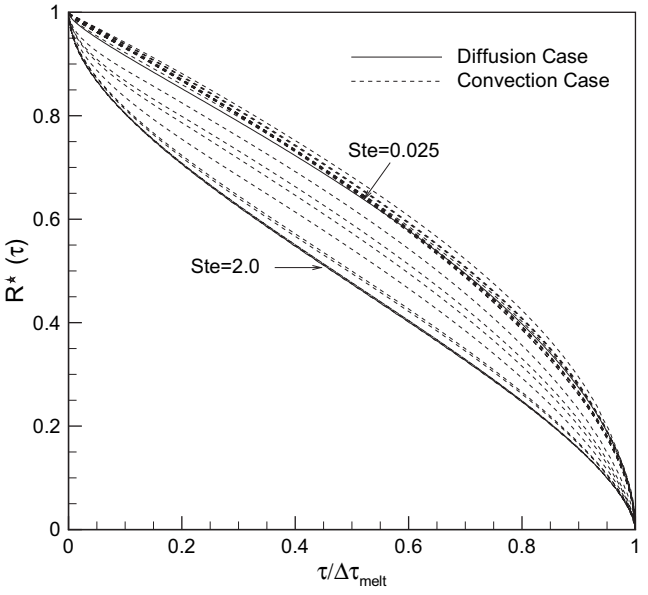

Fig. 8. Effective radius of solid verses fraction total melting time.

3.2.1. Slow flow case, Re = 100

Fig. 9 shows the contours of streamlines and enthalpy fields for Re = 100 and Ste = 0.025 for Pr numbers 0.01, 0.05 and 0.13 at three instances of time – beginning, middle and completion of melting. The top nine plots correspond to streamlines, whereas bottom nine plots are for enthalpy. Forced convection effects can be seen even for Re = 100 as the value for RePr/Ste$^{2/3} > 5$. The fluid flows over the particle and produces a wake in the downstream region. Although the particle remains approximately spherical it is observed that the melting is faster in the upstream region where convection aids conduction heat transfer and slower in the downstream region where clockwise recirculation is visible. The effect of convection can be realised by observing the enthalpy contours which deviate from being concentric rings around the solid particle. The recirculating cell in the downstream region of the solid produces an oval shaped cold plume encompassed by iso-enthalpy contour $h=0.7$. Flow field and heat transfer characteristics changed completely with increase in Stefan number to 2.0 in Fig. 10. Throughout the melting process where the value of RePr/Ste$^{2/3} < 5$, the enthalpy contours are closer to concentric rings indicating the dominance of the conduction mode of heat transfer and the strength of the wake in the downstream region is negligible. For the case of Pr = 0.13 in Fig. 10 the value of RePr/Ste$^{2/3} = 8.2$ and a kidney shaped cold plume appears in the downstream region in the iso-enthalpy plot. Due to high Stefan number of Ste = 2.0 the melting process is mainly driven by conduction heat transfer and the total time of melting decreased by almost fifty-fold as compared to the low Ste = 0.025.

3.2.2. Fast flow case, Re = 1000

Fig. 11 shows the instantaneous contours of streamlines and enthalpy fields for Re = 1000, Ste = 0.025 and Pr = 0.01, 0.05 and 0.13 at the beginning, middle and end of the melting process. As RePr/Ste$^{2/3}$ exceeds 100, the effect of convection can be seen from the beginning of the melting process. The enthalpy contours deviate further from being concentric rings even at the beginning of melting and the solid portion is shaped as oblate spheroid. Even the strength of clockwise rotating recirculating cell increased markedly due to higher Reynolds number and a kidney shaped cold plume bounded by iso-enthalpy contour $h=0.7$ appears in the downstream region as melting progresses. It is interesting to note that melting rate of front and rear region is much faster than the sides. The circulation in the wake region enhances the heat transfer causing the rear portion to become flat. In turn, the flow pattern is also affected.

Fig. 12 shows the instantaneous contours of streamlines and enthalpy fields for Re = 1000 for high Ste = 2.0 and Pr = 0.01, 0.05 and 0.13 for three different instances during the lifetime of the melting particle. With increase in Stefan number to 2.0 at Pr = 0.01 the value of RePr/Ste$^{2/3} = 6.3$ signify strong conduction and the solid remains approximately spherical during melting. But at high Prandtl number of 0.05 and 0.13 the solid does not remain spherical during melting. It can be easily observed from the plots that clockwise recirculating cell grows and sustains a kidney shaped cold plume in the downstream region that elongates as Prandtl number increases.

3.3. Presentation of some calculated values for melting of metals

The magnitude of superheat in °C for iron, nickel and copper corresponding to different Ste is shown in Table 4. It varies from as low as 10 °C to as high as 800 °C. The high values are realistic for cases where metal powder particles are melted by high energy density sources such as lasers or electron beams. To calculate the Nu number we consider a sphere of initial radius $R_0 = 100$ μm of

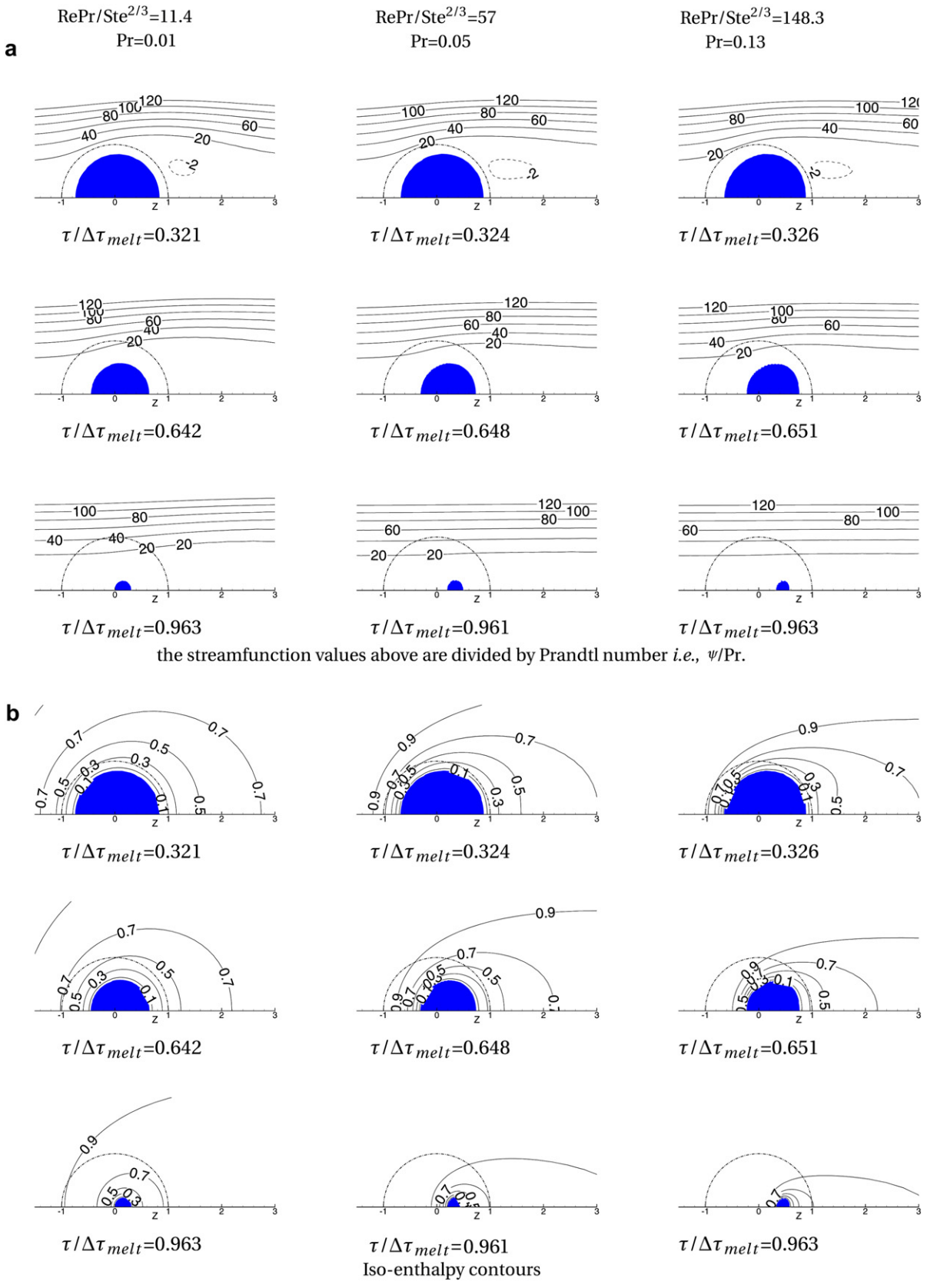

Fig. 9. Streamlines and iso-enthalpy contours for $Re = 1.0 \times 10^2$ and $Ste = 0.025$ at three different instants.

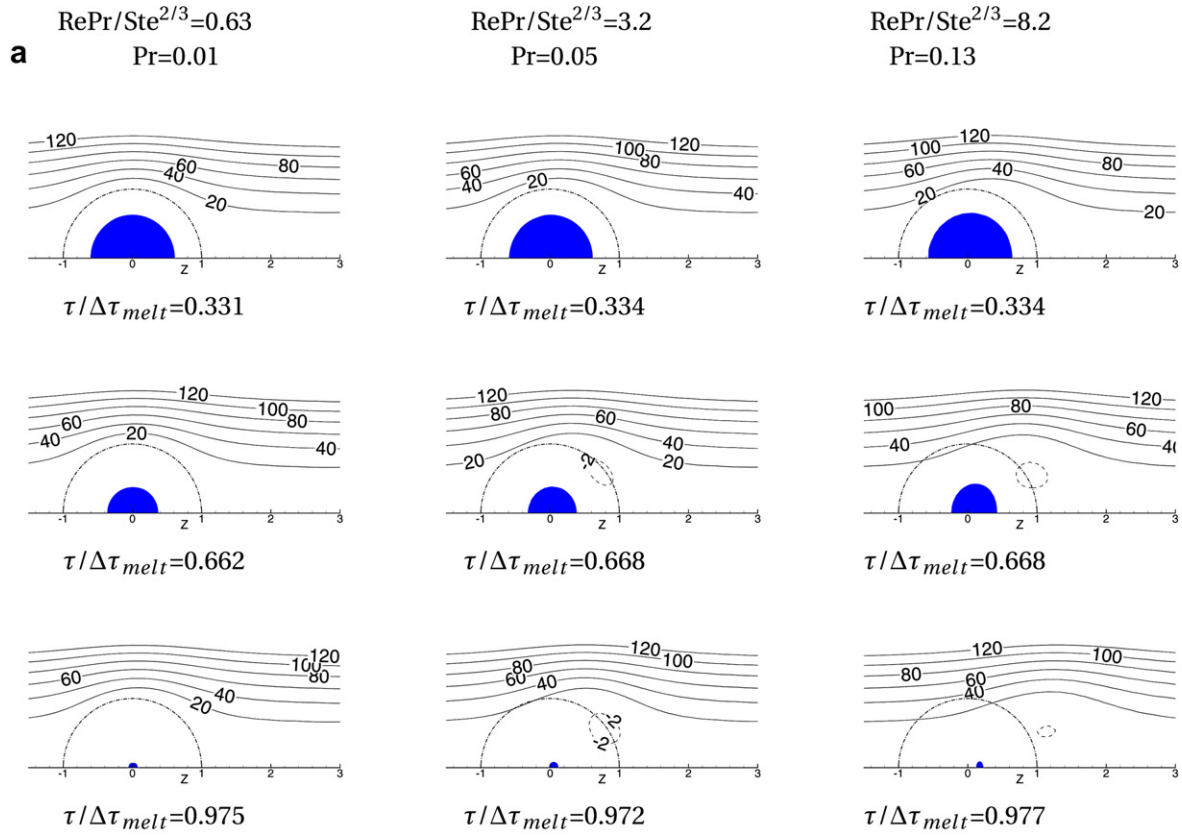

Fig. 10. Streamlines and iso-enthalpy contours for $Re = 1.0 \times 10^2$ and $Ste = 2.0$ at three different instants.

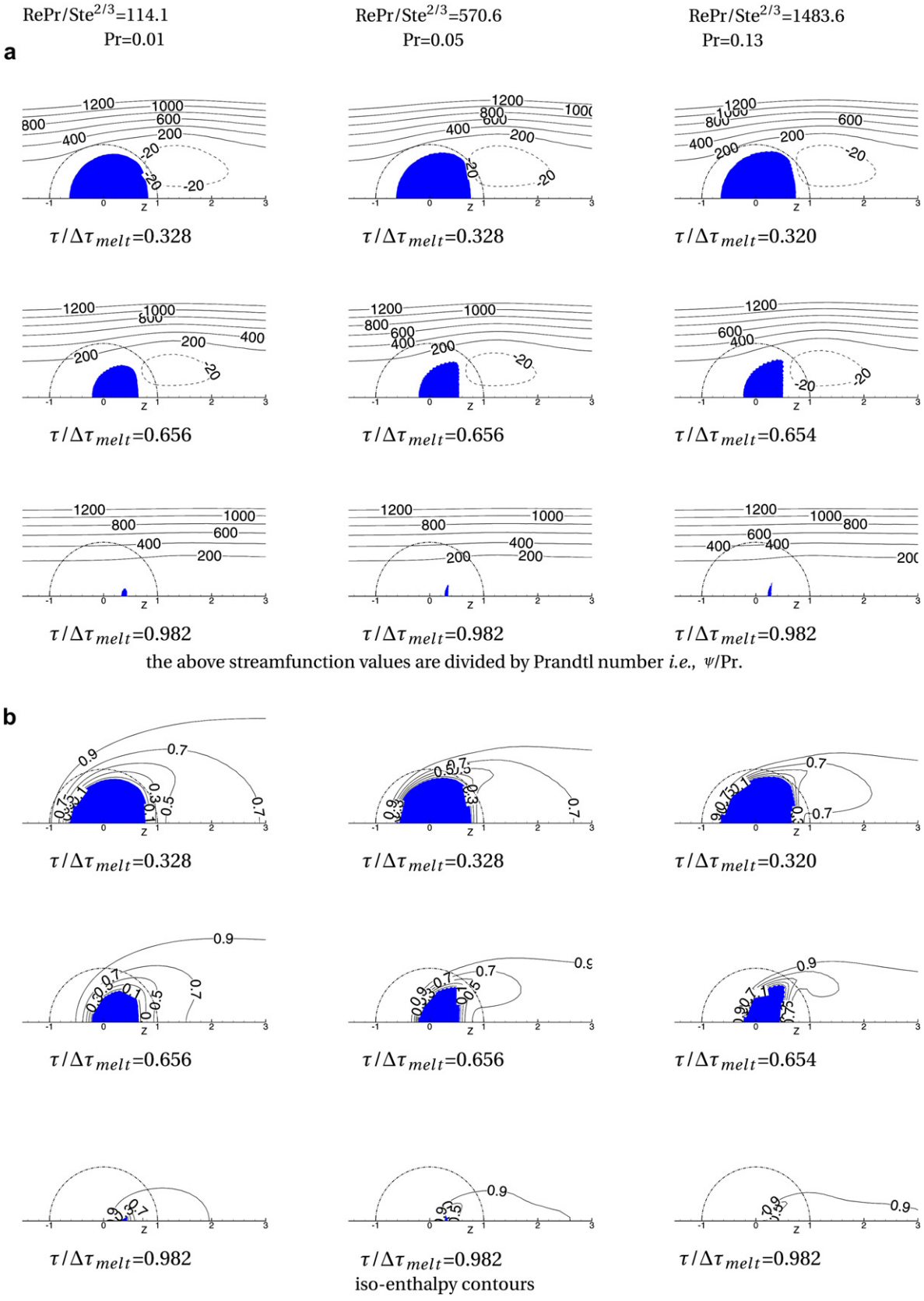

Fig. 11. Streamlines and iso-enthalpy contours for $Re = 1.0 \times 10^3$ and $Ste = 0.025$ at three different instants.

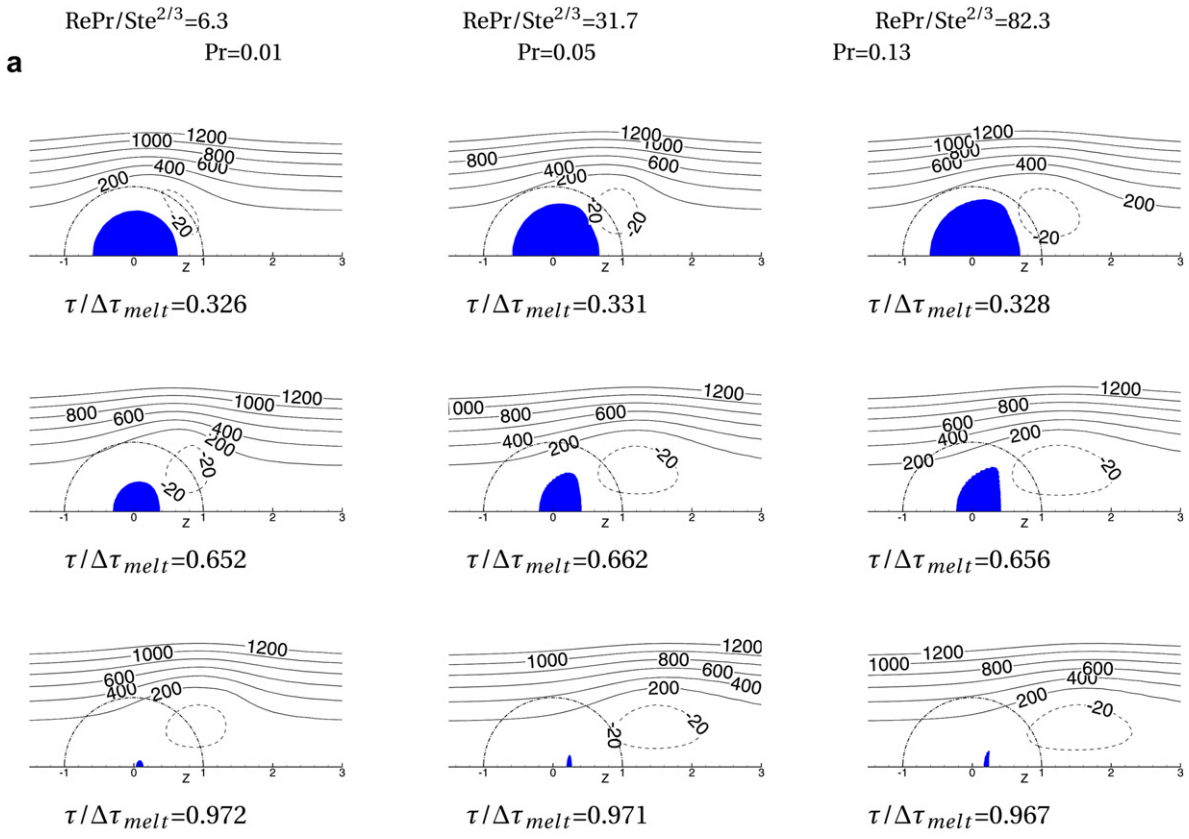

Fig. 12. Streamlines and iso-enthalpy contours for $Re = 1.0 \times 10^3$ and $Ste = 2.0$ at three different instants.

Table 4
Superheat for different metals.

Ste	Superheat ($T - T_l$) in °C		
	Copper (Pr = 0.01)	Nickel (Pr = 0.05)	Iron (Pr = 0.13)
0.025	10.52	10.15	7.50
0.5	210.40	203.00	150.00
2.0	841.60	812.00	600.00

copper, nickel or iron at its melting temperature being injected with a velocity of $U_\infty = 5.025$ m/s into a liquid pool of the same material with a moderate superheat of $(T - T_l) = 100$ °C. The Nusselt number as per the correlation comes out to be equal to 2.7986, 4.8859 and 6.5616 for a Reynolds number of 1000.0, 839.3 and 630.8 for Cu, Ni and Fe respectively.

4. Conclusions

A two-dimensional axisymmetric model is developed to study the heat transfer and fluid flow during melting of a metal spherical particle in its own liquid under forced convective regime for different Prandtl numbers and Stefan numbers. A series of numerical study is carried out to study the combined effects of these parameters on the resultant flow and thermal fields. Some of the important findings of the study may be summarised as follows:

1. A correlation formula for Nusselt number in terms of Prandtl number, Stefan number and Reynolds number for the range $0 \le \mathrm{Re} \le 1.0 \times 10^3$, $0.01 \le \mathrm{Pr} \le 0.13$ and $0.025 \le \mathrm{Ste} \le 2.0$ is

$$\mathrm{Nu} = \frac{2}{3\mathrm{Ste}\Delta\tau_{\mathrm{melt}}} = \left(1.26 + \left(-0.916 + \mathrm{Ste}^{-0.061}\right) \times \mathrm{Re}^{3/4}\mathrm{Pr}^{2/3}\mathrm{Ste}^{1/4}\right)\mathrm{Ste}^{-0.065}$$

2. The dimensionless total time of melting $\Delta\tau_{\mathrm{melt}}$ decreases approximately as $\mathrm{Re}^{3/4}$, $\mathrm{Pr}^{2/3}$ and $\mathrm{Ste}^{5/4}$.
3. The decrease of effective dimensionless radius with fraction of total melting time has been recorded and it is very similar for all the Reynolds number and is close to that of the diffusion-controlled melting.
4. A critical number $\mathrm{RePr}/\mathrm{Ste}^{2/3} \le 5$ is identified below which heat transfer characteristic is mainly governed by diffusion and the spherical particle remains spherical during entire melting process and hence the variation of the effective dimensionless radius with fraction of total melting time becomes similar to the diffusion case. At high $\mathrm{RePr}/\mathrm{Ste}^{2/3}$ as convective heat transfer increases there is more melting in the upstream portion of the solid and the downstream end of the solid becomes flat.

Appendix

Heat transfer coefficient is obtained by performing a heat balance over the time interval, dt, as

$$H_c(h_\infty - h_s) = \rho c L \frac{\mathrm{d}R}{\mathrm{d}t} \tag{8}$$

where all the variables are dimensional.

Here $H_c = H_c(R)$ is the instantaneous heat transfer coefficient for the particle. Assuming that the Nusselt number can be expressed as the function of the Reynolds number [14] we obtain

$$\begin{aligned} &\mathrm{Nu} \propto \mathrm{Re}^{1/2} \\ &\text{and,}\quad H_c \propto \frac{1}{\sqrt{R}} \\ &H_c(R) = H_{c0}\sqrt{R_0}\frac{1}{\sqrt{R}} \end{aligned} \tag{9}$$

where H_{c0} is the heat transfer coefficient for the initial sphere of radius R_0 at time $t = 0$. Substituting H_c from equation (9) into equation (8) and integrating from initial radius R_0 to zero over the time interval Δt_{melt} we get the Nusselt number as:

$$\frac{\int_{R_0}^{0} \sqrt{R}\,\mathrm{d}R}{H_{c0}\sqrt{R_0}} = \frac{\alpha(h_\infty - h_s)}{kL}\int_0^{\Delta t_{\mathrm{melt}}} \mathrm{d}t$$

$$\frac{2R_0}{3H_{c0}} = \frac{\alpha(h_\infty - h_s)}{kL}\Delta t_{\mathrm{melt}}$$

$$\mathrm{Nu} = \frac{H_{c0}R_0}{k} = \frac{2}{3\mathrm{Ste}\Delta t_{\mathrm{melt}}}$$

where $\Delta\tau_{\mathrm{melt}}$ is the non-dimensional total time of melting for the particle with initial radius R_0.

References

[1] A. Kranse, J. Schenk, Thermal free convection from a solid sphere, Applied Scientific Research A 15 (1965) 397–403.
[2] J. Schenk, F.M. Schenkels, Thermal free convection from an ice sphere in water, Applied Scientific Research 19 (1968) 465–476.
[3] P. Mcleod, D. Riley, R. Sparks, Melting of a sphere in hot fluid, Journal of Fluid Mechanics 327 (1996) 393–409.
[4] Y.L. Hao, Y.X. Tao, Melting of a solid sphere under forced and mixed convection: flow characteristics, ASME Journal of Heat Transfer 123 (2001) 937–950.
[5] Y.L. Hao, Y.X. Tao, Heat transfer characteristics of melting ice spheres under forced and mixed convection, ASME Journal of Heat Transfer 124 (2002) 891–903.
[6] F. Kreith, L.G. Roberts, J.A. Sullivan, S.N. Sinha, Convection heat transfer and flow phenomena of rotating spheres, International Journal of Heat and Mass Transfer 6 (1963) 881–895.
[7] C. Hsu, Heat transfer to liquid metals flowing past spheres and elliptical-rod bundles, International Journal of Heat and Mass Transfer 8 (1965) 303–315.
[8] A. Anselmo, V. Prasad, J. Koziol, K.P. Gupta, Numerical and experimental study of a solid pellet feed continuous Czochralski growth process for silicon single crystal, Journal of Crystal Growth 131 (1993) 247–264.
[9] S. Argyropoulos, A. Mikrovas, An experimental investigation on natural and forced convection in liquid metals, International Journal of Heat and Mass Transfer 39 (1996) 547–561.
[10] S. Argyropoulos, A. Mikrovas, D.A. Doutre, Dimensionless correlations for forced convection in liquid metals. Part I: single-phase flow, Metallurgical and Materials Transaction 32B (2001) 239–246.
[11] B. Melissari, S. Argyropoulos, Measurement of magnitude and direction of velocity in high-temperature liquid metals. Part I: mathematical modeling, Metallurgical and Materials Transaction 36B (5) (2005a) 691–700.
[12] B. Melissari, S. Argyropoulos, Measurement of magnitude and direction of velocity in high-temperature liquid metals. Part II: experimental measurements, Metallurgical and Materials Transactions 36B (5) (2005b) 639–649.
[13] B. Melissari, S. Argyropoulos, Development of a heat transfer dimensionless correlation for spheres immersed in a wide range of Prandtl number fluids, International Journal of Heat and Mass Transfer 48 (2005c) 4333–4341.
[14] H. Schlichting, Boundary Layer Theory, seventh ed. McGraw-Hill, New York, NY, 1979.
[15] V.R. Voller, C. Prakash, A fixed grid numerical modelling methodology for convection-diffusion mushy-region phase change problems, International Journal of Heat and Mass Transfer 30 (8) (1987) 1709–1719.
[16] X.K. Lan, J.M. Khodadadi, Fluid flow, heat transfer and solidification in the mold of continuous casters during ladle change, International Journal of Heat and Mass Transfer 44 (2001) 953–965.
[17] S.V. Patankar, Numerical Heat Transfer and Fluid Flow, Hemisphere Publishing, Washington DC, 1980.
[18] J.H. Ferziger, M. Peric, Computational Methods for Fluid Dynamics, second ed. Springer-Verlag, Berlin Heidelberg, Germany, 1999.
[19] S. Kakac, Y. Yener, Heat Conduction, Hemisphere Publishing Corporation, 1985.
[20] K.C. Mills, Recommended Values of Thermo-physical Properties for Selected Commercial Alloys, Woodhead Publishing Limited, Cambridge England, 2002.
[21] A. Brandes, G.B. Brook, Smithells Metals Reference Book, seventh ed. Butterworth Heinemann, 1998.